

Low-momentum ring diagrams of neutron matter at and near the unitary limit

L.-W. Siu, T. T. S. Kuo

Department of Physics and Astronomy, Stony Brook University, NY 11794-3800, USA

R. Machleidt

Department of Physics and Astronomy, University of Idaho, Moscow, ID 83844, USA

We study neutron matter at and near the unitary limit using a low-momentum ring diagram approach. By slightly tuning the meson-exchange CD-Bonn potential, neutron-neutron potentials with various 1S_0 scattering lengths such as $a_s = -12070 fm$ and $+21 fm$ are constructed. Such potentials are renormalized with rigorous procedures to give the corresponding a_s -equivalent low-momentum potentials V_{low-k} , with which the low-momentum particle-particle hole-hole ring diagrams are summed up to all orders, giving the ground state energy E_0 of neutron matter for various scattering lengths. At the limit of $a_s \rightarrow \pm\infty$, our calculated ratio of E_0 to that of the non-interacting case is found remarkably close to a constant of 0.44 over a wide range of Fermi-momenta. This result reveals an universality that is well consistent with the recent experimental and Monte-Carlo computational study on low-density cold Fermi gas at the unitary limit. The overall behavior of this ratio obtained with various scattering lengths is presented and discussed. Ring-diagram results obtained with V_{low-k} and those with G -matrix interactions are compared.

PACS numbers: pacs

I. INTRODUCTION

Back in 1999, Bertsch[1] formulated a many-body problem, asking: what are the ground state properties of a two-species fermion system that has a zero-range interaction and an infinite scattering length? Such problem was originally set up as a parameter-free model for a fictitious neutron matter. Recently, as the experiments on trapped cold alkali gas undergo huge breakthroughs, degenerate Fermi gas with a tunable scattering length (including $\pm\infty$) becomes accessible in laboratories[2]. Since then cold Fermi systems have aroused growing attention.

The term ‘unitary limit’ has been used by many authors to refer to the special scenario in a low-density two-species many-body system where the scattering length between particles approaches infinity. More specifically, at the unitary limit, the scattering length a_s , the Fermi momentum k_F , and the range of the interaction r_{int} satisfy $|a_s| \gg k_F^{-1} \gg r_{int}$. Under such condition, atoms are ‘strongly interacting’, and a full theoretical description of their properties is a challenging task in many-body theory. Universal behavior is expected to show up in various aspects, including ground state properties as discussed below, collective excitations [3, 4, 5, 6, 7, 8, 9], and thermodynamic properties [10, 11, 12, 13, 24]. Such universality can be naively understood as the ‘dropping’ of the scattering length a_s out of the problem, leaving k_F as the only relevant length scale. In particular, the ground state energy E_0 , is expected to be proportional to that of the non-interacting gas E_0^{free} [14], that is $E_0/E_0^{free} = \xi$, or equivalently

$$\frac{E_0}{A} = \frac{3}{5} \frac{k_F^2}{2} \xi \quad (1)$$

($\hbar = m = 1$), A being the number of particles. The universal constant ξ is of great interest and many attempts have been made to derive it analytically or determine it experimentally.

Theoretical calculations suggest that ξ is between 0.3 to 0.7. For example, an early work based on different Padé approximations gives $\xi = 0.326, 0.568$ [14]. Diagrammatic approach gives 0.326 with Galitskii resummation[15], 0.7 with ladder approximation[15], and 0.455 with a diagrammatic BCS-BEC crossover theory[17]. Other theoretical approaches have also been used, including ϵ expansion, which gives $\xi=0.475$ in [18] and [20], and variational formalism, which gives 0.360 in [19]. The four most recent experimental measurements are listed in Table I. Though the experimental results are consistent with each other, the experimentally determined value of ξ still falls between relatively large error bars($\sim 10\%$). By far the best estimate on ξ is considered to be that from Quantum Monte-Carlo methods, giving $\xi = 0.44(1)$ [21] and $0.42(1)$ [22].

ξ	Authors	Ref.
0.36(15)	Bourdel <i>et.al</i>	[23]
0.51(4)	Kinast <i>et.al</i>	[24]
0.46(5)	Partridge <i>et.al</i>	[25]
$0.46^{+0.05}_{-0.12}$	Stewart <i>et.al</i>	[26]

TABLE I: Comparison of recent experimental values on ξ .

Cold and dilute neutron matter is a special class of cold Fermi system with great importance in astrophysics. Its properties at resonance has attracted much interest recently [27, 28]. In this work we report results from low-momentum ring diagram calculations on the ground-state energy of neutron matter at and near the

unitary limit. As is well-known, the 1S_0 channel of neutron matter has a fairly large scattering length a_s ($-18.97fm$), nonetheless, it is still finite. Here, by adjusting the interaction parameters of the CD-Bonn potential [29], we construct ‘tuned’ neutron interactions with different a_s ’s such as $-9.83fm$, $-12070fm$ and $+21fm$ (which possesses a bound state). For a wide range of neutron density, the case of $a_s = -12070fm$ can be considered the same as the unitary limit, namely $a_s \rightarrow -\infty$. We shall compute the ground state energy of neutron matter, with inter-neutron potentials being these ‘tuned’ CD-Bonn’s, by two steps: renormalization followed by ring summation. We first renormalize neutron interactions with a T-matrix equivalence renormalization method [30, 31, 32, 33, 34, 36], where the high-momentum components beyond a decimation scale Λ are integrated out. This gives the corresponding low-momentum interactions V_{low-k} ’s with the scattering lengths being preserved. Then, we calculate the ground state energy by summing the particle-particle-hole-hole ($pphh$) ring diagrams[37] to all orders. In such ring summation, we employ a model space approach, namely, the summation is carried out within a model space characterized by $\{k \leq \Lambda\}$.

We shall closely examine how our results differ from similar calculations with a different renormalized interaction - the Brueckner G -matrix on which the Brueckner Hartree-Fock(BHF) method is based. The BHF method has been widely used for treating the strongly interacting nuclear many body problems [38, 39]. However, BHF is a lowest-order reaction matrix (G -matrix) theory and may be improved in several aspects. To take care of the short range correlations, the ladder diagrams of two particles interacting with the bare interaction are summed to all orders in BHF. However, this method does not include diagrams representing hole-hole correlations such as diagram (iii) of Fig.1. Note that this diagram has repeated ($pphh$) interactions as well as self-energy insertions to both hole and particle lines. Another aspect of the traditional BHF is that it employs a discontinuous single-particle (s.p.) spectrum which has a gap at the Fermi surface k_F . To improve upon these drawbacks, Song et al. [37] have formulated a G -matrix ring-diagram method for nuclear matter, with which the $pphh$ ring diagrams such as diagrams (i) to (iii) of Fig.1 are summed to all orders. This ring-diagram method has been applied to nuclear matter and given satisfactory result [37]. The V_{low-k} ring diagram method used in this work is highly similar to [37]’s, except for one significant difference: the interaction used in the G -matrix ring diagram method is energy dependent. (The Brueckner G -matrix is energy dependent, as we shall later discuss.) This complicates the calculation a lot. V_{low-k} provides a cleaner and simpler implementation on such all-order ring summation.

We shall first provide an outline of the ring-diagram approach in section II. The derivation details of the low-momentum interaction from the CD-Bonn potentials shall be followed in section III. Our major results from

the V_{low-k} ring diagram method are in section IV. There we shall present our results for the ground-state energy and ratio E_0/E_0^{free} obtained with potentials of various scattering lengths. A fixed-point criterion for determining the decimation scale Λ will be discussed. There one can also find a comparison of data on the ground state energy obtained with two different methods-the V_{low-k} and the G -matrix ring diagram methods. We shall summarize and discuss our work in the last section.

II. LOW-MOMENTUM RING DIAGRAMS

In this section we describe how we calculate the ring diagrams for the ground state energy shift ΔE_0 , which is defined as the difference $(E_0 - E_0^{free})$ where E_0 is the true ground-state energy and E_0^{free} is the corresponding quantity for the non-interacting system. In the present work, we consider the $pphh$ ring diagrams as shown in Fig. 1. We shall calculate the all-order sum, denoted as ΔE_0^{pp} , of such diagrams. Our calculation is carried out within a low-momentum model space $\{k \leq \Lambda\}$ and each vertex of the diagrams is the renormalized effective interaction corresponding to this model space. Two types of such interactions will be employed, one being the energy-independent V_{low-k} and the other being the energy-dependent G -matrix interaction. Let us consider first the former. In this case, ΔE_0^{pp} can be written [37] as

$$\Delta E_0^{pp} = \frac{-1}{2\pi i} \int_{-\infty}^{\infty} d\omega e^{i\omega 0^+} \text{tr}_{<\Lambda} [F(\omega) V_{low-k} + \frac{1}{2}(F(\omega) V_{low-k})^2 + \frac{1}{3}(F(\omega) V_{low-k})^3 + \dots] \quad (2)$$

where F is the free $pphh$ propagator

$$F_{ab}(\omega) = \frac{\bar{n}_a \bar{n}_b}{\omega - (\epsilon_a + \epsilon_b) + i0^+} - \frac{n_a n_b}{\omega - (\epsilon_a + \epsilon_b) - i0^+} \quad (3)$$

with $n_a = 1$, $a \leq k_F$; $= 0$, $k > k_F$ and $\bar{n}_a = (1 - n_a)$.

We now introduce a strength parameter λ and a λ -dependent Green function $G^{pp}(\omega, \lambda)$ defined by

$$G^{pp}(\omega, \lambda) = F(\omega) + \lambda F(\omega) V_{low-k} G^{pp}(\omega, \lambda). \quad (4)$$

The energy shift then takes the following simple form when expressed in terms of G^{pp} , namely

$$\Delta E_0^{pp} = \frac{-1}{2\pi i} \int_0^1 d\lambda \int_{-\infty}^{\infty} e^{i\omega 0^+} \text{tr}_{<\Lambda} [G^{pp}(\omega, \lambda) V_{low-k}] \quad (5)$$

Using Lehmann’s representation for G^{pp} , one can show that

$$\Delta E_0^{pp} = \int_0^1 d\lambda \sum_m \sum_{ijkl < \Lambda} Y_m(ij, \lambda) Y_m^*(kl, \lambda) \langle ij | V_{low-k} | kl \rangle, \quad (6)$$

where the transition amplitudes Y are given by the following RPA equation:

$$\sum_{ef} [(\epsilon_i + \epsilon_j)\delta_{ij,ef} + \lambda(1 - n_i - n_j)\langle ij|V_{low-k}|ef\rangle] \times Y_m(ef, \lambda) = \omega_m Y_m(ij, \lambda); \quad (i, j, e, f) < \Lambda. \quad (7)$$

The index m denotes states dominated by hole-hole components, namely, states that satisfy $\langle Y_m | \frac{1}{Q} | Y_m \rangle = -1$ and $Q(i, j) = (1 - n_i - n_j)$. We have used the HF s.p. spectrum given by V_{low-k} , namely

$$\epsilon_k = \hbar^2 k^2 / 2m + \sum_{h < k_F} \langle kh | V_{low-k} | kh \rangle \quad (8)$$

for both holes and particles with $k \leq \Lambda$. Thus the propagators of the diagrams as shown in Fig. 1 all include HF insertions to all orders. The above spectrum is continuous up to Λ .

The above ring-diagram method is a renormalization group approach for a momentum model space defined by a momentum boundary Λ , and the space with momentum greater than Λ is integrated out. The resulting effective interaction for the model space is V_{low-k} which is energy independent. This renormalization procedure can, however, also lead to a model-space effective interaction which is energy dependent. The G -matrix ring-diagram method of [37] is of the latter approach. Formally, these two approaches should be the same. In the present work we shall carry out ring-diagram calculations using both approaches; it would be of interest to compare the results of these two different approaches.

In the following, let us briefly describe the G -matrix ring diagram method [37]. Here each vertex of Fig. 1 is a model-space G -matrix interaction, to be denoted as G^M . It is defined by

$$G_{ijkl}^M(\omega) = V_{ijkl} + \sum_{rs} V_{ijrs} \frac{Q^M(rs)}{\omega - k_r^2 - k_s^2 + i0^+} G_{rskl}^M(\omega) \quad (9)$$

where k_r^2 stands for the kinetic energy $\hbar^2 k_r^2 / 2m$ and similarly for k_s^2 . The Pauli projection operator Q^M is to assure the intermediate states being outside Λ and k_F , namely it is defined by

$$Q^M(rs) = 1, \text{ if } \max(k_r, k_s) > \Lambda \text{ and } \min(k_r, k_s) < k_F \\ = 0, \text{ otherwise.} \quad (10)$$

In the above $k_F < \Lambda$. In Ref.[37] Λ is chosen to be $\sim 3fm^{-1}$. Note that the above G^M is energy dependent, namely it is dependent on the energy variable ω . However, ω is not a free parameter; it is to be determined in a self-consistent way. For example, the model-space s.p. spectrum is given by the following self-consistent equations:

$$\epsilon_a = \frac{\hbar^2 k_a^2}{2m} + \langle a | U | a \rangle; \quad (11)$$

$$\langle a | U | a \rangle = \sum_{h \leq k_F} \langle a, h | G^M(\omega = \epsilon_a + \epsilon_h) | a, h \rangle, \quad a < \Lambda \\ = 0, \text{ otherwise.} \quad (12)$$

In the above U is the s.p. potential and ϵ the model-space s.p. energy which is determined self-consistently with the energy variable of G^M . Note that this s.p. spectrum does not have a gap at k_F ; it is a continuous one up to Λ . When choosing $\Lambda = k_F$ the above is the same as the self-consistent BHF s.p. spectrum.

When calculating the ring diagrams using G^M , its energy variable is also determined self-consistently. In terms of G^M , the all-order sum of the $pphh$ ring diagrams is [37]

$$\Delta E_0^{pp} = \int_0^1 d\lambda \sum_m \sum_{ijkl(<\Lambda)} Y_m(ij, \lambda) Y_m^*(kl, \lambda) G_{kl,ij}^M(\omega_m^-) \quad (13)$$

where the transition amplitudes Y_m and eigenvalues ω_m^- are given by the following self-consistent RPA equation:

$$\sum_{ef} [(\epsilon_i + \epsilon_j)\delta_{ij,ef} + \lambda(1 - n_i - n_j)L_{ij,ef}(\omega)] Y_m(ef, \lambda) \\ = \mu_m(\omega, \lambda) Y_m(ij, \lambda); \quad (i, j, e, f) < \Lambda. \quad (14)$$

The index m denotes states dominated by hole-hole components. The vertex function L is obtained from 2- and 1-body diagrams first order in G^M [37]. The above equation is solved with the self-consistent condition that the energy variable of L is equal to the eigenvalue, namely

$$\omega = \mu_m(\omega, \lambda) \equiv \omega_m^-(\lambda). \quad (15)$$

Comparing with the V_{low-k} ring diagram calculation described earlier, the above G -matrix calculation is clearly more complicated. Because of the energy dependence of the interaction G^M , the above equations have to be solved self-consistently both for the s.p. spectrum and for the RPA equations. To attain this self consistency, it is necessary to use iteration methods and this procedure is often numerically involved. In contrast, ring-diagram calculation using the energy-independent interaction V_{low-k} is indeed much simpler. As mentioned earlier, we shall carry out ring-diagram calculations using both methods.

III. V_{low-k} WITH INFINITE SCATTERING LENGTH

To carry out the above ring-diagram calculation, we need the low-momentum potential V_{low-k} . Since we are interested at neutron matter at and near the unitary limit (infinite scattering length), we should have V_{low-k} 's of definite scattering lengths, including $\pm\infty$, so that the dependence of our results on scattering lengths can be investigated. In the present work, we have chosen a two-step procedure to construct such potentials so that the resulting potentials are close to realistic neutron potentials.

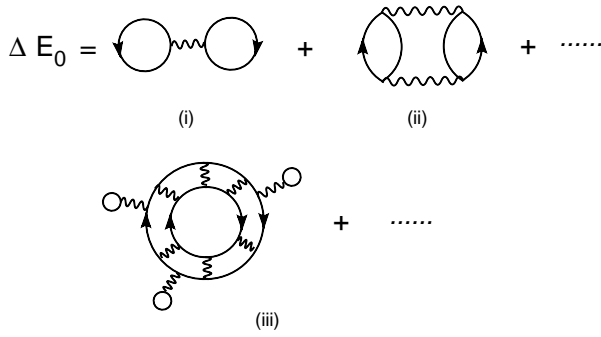


FIG. 1: $pphh$ ring-diagram summation in the calculation of the ground state energy shift.

We first construct bare potentials V^a based on a realistic nucleon-nucleon potential; these potentials are tuned so that they have definite scattering lengths. Renormalized low-momentum potentials V_{low-k}^a are then obtained from V^a using a renormalization procedure which preserves the scattering length.

We start from the high-precision CD-Bonn [29] nucleon-nucleon potential. For this potential, the scattering length of the 1S_0 channel is already fairly large ($-18.97 fm$), and it is found to depend rather sensitively on the interaction parameters. Thus by slightly tuning the interaction parameters of the CD-Bonn potential, we have obtained a family of 1S_0 neutron potentials of definite scattering lengths. We shall denote them as V^a . Our tuning procedure will be discussed in section IV(A).

Recently there have been a number of studies on the low-momentum nucleon-nucleon potential V_{low-k} [30, 31, 32, 33, 34, 36]. V_{low-k} is obtained from a bare nucleon-nucleon potential by integrating out the high-momentum components, under the restriction that the deuteron binding energy and the low-energy phase-shifts are preserved. The V_{low-k} obtained from different realistic potentials (CD-Bonn [29], Argonne [40], Nijmegen [41] and Idaho [42]) all flow to a unique potential when the cut-off momentum is lowered to around $2fm^{-1}$. The above V_{low-k} is obtained using a T-matrix equivalence renormalization procedure [30, 31, 32, 33, 34, 36]. Since this procedure preserves the half-on-shell T-matrix, it of course preserves the scattering length. Thus this procedure is suitable for constructing V_{low-k}^a , the low-momentum interaction with definite scattering length. Using this procedure, we start from the T-matrix equation

$$T(k', k, k^2) = V^a(k', k) + \int_0^\infty q^2 dq \frac{V^a(k', q)T(q, k, k^2)}{k^2 - q^2 + i0^+}, \quad (16)$$

where V^a is a modified CD-Bonn potential of scattering length a . Notice that in the above the intermediate state momentum q is integrated from 0 to ∞ . We then define

an effective low-momentum T-matrix by

$$T_{low-k}(p', p, p^2) = V_{low-k}^a(p', p) + \int_0^\Lambda q^2 dq \frac{V_{low-k}^a(p', q)T_{low-k}(q, p, p^2)}{p^2 - q^2 + i0^+}, \quad (17)$$

where the intermediate state momentum is integrated from 0 to Λ , the momentum space cut-off. We require the above T-matrices to satisfy the condition

$$T(p', p, p^2) = T_{low-k}(p', p, p^2); \quad (p', p) \leq \Lambda. \quad (18)$$

The above equations define the effective low momentum interaction V_{low-k}^a . The iteration method of Lee-Suzuki-Andreozzi [43, 44] has been used in calculating V_{low-k}^a from the above T-matrix equivalence equations. From now on, we shall denote V_{low-k}^a simply as V_{low-k} .

IV. RESULTS

A. Low-momentum interactions and scattering lengths

To study neutron matter at the unitary limit, we first need a realistic neutron-neutron interaction that would lead to a huge 1S_0 scattering length a_s , and a small effective range r_e . We obtain such interaction by ‘tuning’ the meson mass m_σ in the usual CD-Bonn potential. The exchange of a lighter meson generates a stronger attraction, therefore making the scattering length a_s more negative until a bound state is formed. As one ‘tunes’ across the bound state, a_s will pass from $-\infty$ to $+\infty$, eventually become less and less positive. In this work, this m_σ ‘tuning’ is taken as a manual adjustment in the strength of the neutron-neutron potential. Of great interest is that this ‘tuning’ may naturally come from the density-dependence of the nucleon-nucleon potential via the mechanism of Brown-Rho (BR) scaling[45, 46, 47], which suggests the in-medium meson masses should *decrease*.

At normal nuclear matter density, the meson masses of ρ , ω and σ are all expected to decrease by about 15% [47] compared to their masses in free space. This decrease will enhance not only the attraction from σ but also the repulsion from ρ and ω . As a preliminary study, we shall tune only m_σ in the present work. To compensate for the repulsive effect from ρ and ω (which are not tuned in the present work), we shall only tune m_σ slightly, namely a few percent. We shall consider that the above BR scaling is compatible with neutron matter of moderate density ($k_F \sim 1fm^{-1}$). In a future publication, we plan to carry out further studies, including the tuning of ρ - and ω -meson masses.

Various ‘tuned’ CD-Bonn potentials are listed in Table II. From there one can see the sensitivity of the scattering length to the change in m_σ . At $m_\sigma \approx 442MeV$, namely a

name	$m_\sigma(\text{MeV})$	$a_s(\text{fm})$	$r_e(\text{fm})$
original CD-Bonn	452	-18.97	2.82
CD-Bonn-10	460	-9.827	3.11
CD-Bonn-42	447	-42.52	2.66
CD-Bonn- ∞	442.85	-12070.00	2.54
CD-Bonn+ ∞	442.80	+5121.00	2.54
CD-Bonn+21	434	+21.01	2.31

TABLE II: m_σ in the original CD-Bonn potential is tuned to give neutron-neutron potentials with different scattering lengths.

2.4% decrease from the original, $a_s \approx -12000\text{fm}$. Notice that the effective ranges for the CD-Bonn potentials are larger than the actual ranges of them. For example, r_e for the original CD-Bonn potential is 2.82fm , considerably larger than the range of one-pion exchange. Within the range of Fermi momenta from 0.8fm^{-1} to 1.5fm^{-1} that we use in our computation below, $a_s \approx -12000\text{fm}$ is obviously enormous compared to any length scale in the system, thus we expect the neutron matter to be at the unitary limit, i.e., no different from the limiting case $a_s = -\infty$. For convenience, we name such potential CD-Bonn- ∞ .

Following the renormalization procedures as already described in Section III, we obtain the low-momentum potential V_{low-k} 's for several CD-Bonn potentials listed above. A comparison of the diagonal matrix elements in the V_{low-k} 's (with a fixed cut-off momentum Λ) is shown in Figure 2. It is of interest that the strength of V_{low-k} only changes weakly with the scattering length. For example, it changes by merely about 10% from $a_s = -18.97\text{fm}$ to -12070fm .

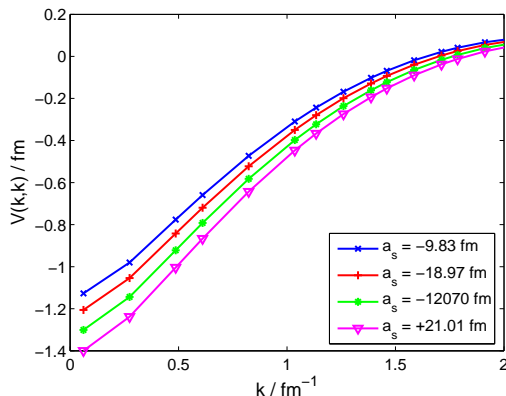


FIG. 2: Diagonal matrix elements of V_{low-k} constructed from CD-Bonn potentials with different scattering lengths. $\Lambda = 2.4\text{fm}^{-1}$ is used in all cases.

B. Ground-state energy and

the universal constant ξ

Here we shall present our major results, namely the ground state energies E_0 of neutron matter at and close to the unitary limit from the summation of low-momentum ring diagrams to all orders. Following the potential renormalization procedure described in section III, we first calculate V_{low-k} for certain chosen values for the decimation scale Λ . Then the all-order sum of the $pphh$ ring diagrams are calculated using the above V_{low-k} . As introduced in Section II, the calculation details in the summation of $pphh$ ring diagrams can be found in Ref.[37]. How to choose the decimation scale Λ is clearly an important step in our calculation, and in the present work we shall use a stable-point, or ‘fixed-point’, criterion in deciding Λ . Before discussing this criterion, let us first present some of our results for the ground-state energy per particle (E_0/A). In Fig. 3 we present such results for four a_s values, calculated with Λ s determined by the above criterion. (The details of this determination will be described a little later.) As shown by the figure, we see that E_0/A does not change strongly with a_s . The ratios $\xi = E_0/E_0^{free}$ are then readily obtained, as shown in Fig.4. It is of interest that the ratios for the four a_s cases are all weakly dependent on k_F . To help understand this behavior, we plot in Fig.5 the potential energy per particle PE/A (namely $\Delta E_0^{pp}/A$ of Eq.(6)) versus k_F^2 , for the same four a_s cases. It is rather impressive that they all appear to be straight lines. We have fitted the ‘lines’ in the figure to the equation $PE/A = (\hbar^2/m)(\beta k_F^2 + \gamma)$: We have found $(\beta, \gamma) = (-0.1370, 0.0002)$, $(-0.1498, -0.0008)$, $(-0.1649, -0.0035)$ and $(-0.1797, -0.0082)$ respectively for $a_s = -9.87\text{fm}$, -18.97fm , -12070fm and $+21.0\text{fm}$. The rms deviation for the above fitting are all very small (all less than 0.0013), confirming that they are indeed very close to straight lines. The above results are of interest, and are consistent with those shown in Fig. 4. In fact the ratios of Fig.4 are determined by the ‘slopes’ of these ‘lines’.

Before further discussing our results, let us now address the question of how to determine the decimation scale Λ . There are basically two considerations: The first one concerns the experimental NN scattering phase shifts on which realistic NN potentials are based. The second is about the dependence of our results on Λ . Realistic NN potentials [29, 40, 41, 42] are constructed to reproduce the experimental NN phase shifts up to $E_{lab} \approx 300\text{MeV}$. This suggests that Λ is about 2fm^{-1} , as beyond this scale NN potential models are not experimentally constrained and are thus rather uncertain (model dependent) [34].

We now turn to the dependence of our results on Λ . As described in Section II, V_{low-k} is used in the determination of the H.F. single particle spectrum (see Eq.8), the transition amplitudes Y in the RPA equation (see Eq.7), and finally, the ground state energy E_0 (see Eq. 6). Intuitively, E_0 should exhibit a non-trivial Λ -dependence. For various Fermi-momenta, this dependence is studied and is found to be remarkably mild.

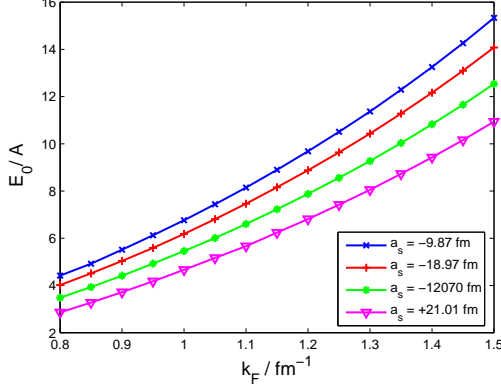


FIG. 3: Ground state energy per particle, E_0/A , of neutron matter with various tuned CD-Bonn potentials, computed from the summation of low-momentum $pphh$ ring diagrams. Only 1S_0 contribution is included.

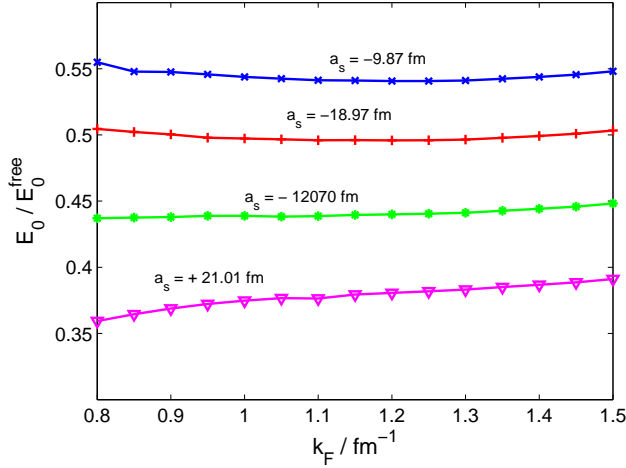


FIG. 4: The ratio E_0/E_0^{free} as a function of Fermi momentum k_F for the various CD-Bonn potentials listed in Table II. The data with CD-Bonn- ∞ ($a_s = -12070 fm$) indicates that E_0/E_0^{free} is a constant of 0.443 ± 0.006 over the range of k_F as shown.

As an example, let us present in Fig. 6 our results obtained with the potential CD-Bonn- ∞ . For $\Lambda = (2.0 - 2.6) fm^{-1}$, it is seen that ξ varies actually by a rather small amount (note that the range of our plot is from 0.438 to 0.444). Furthermore the Λ dependence of ξ shows up as a curve with a minimum. The final choice of Λ is based on the criterion that E_0 should be stable against changes in Λ . As shown in the figure, an obvious stable-point, or fixed-point, defined by $dE_0(\Lambda)/d\Lambda = 0$, is found at about $2.3 fm^{-1}$. Thus we have used $\Lambda = 2.3 fm^{-1}$ for CD-Bonn- ∞ . We found that the position of the fixed point is almost the same for the different Fermi-momenta in the range $(0.8 - 1.5) fm^{-1}$. The same procedure is done on the original CD-Bonn,

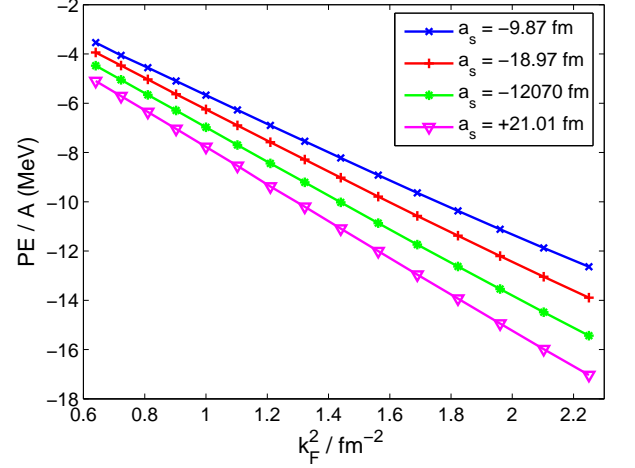


FIG. 5: Potential energy per particle, PE/A , of neutron matter with various tuned CD-Bonn potentials, computed from the summation of low-momentum $pphh$ ring diagrams. Only 1S_0 contribution is included.

and other tuned potentials. The fixed points, also with an negligible dependence on k_F , are found to be $2.15 fm^{-1}$, $2.25 fm^{-1}$ and $2.4 fm^{-1}$ respectively for CD-Bonn potentials of scattering lengths $-9.8 fm$, $-18.9 fm$ (the original CD-Bonn), and $+21.01 fm$. The above fixed-point Λ 's have been used for the results presented in Figs. 3-5.

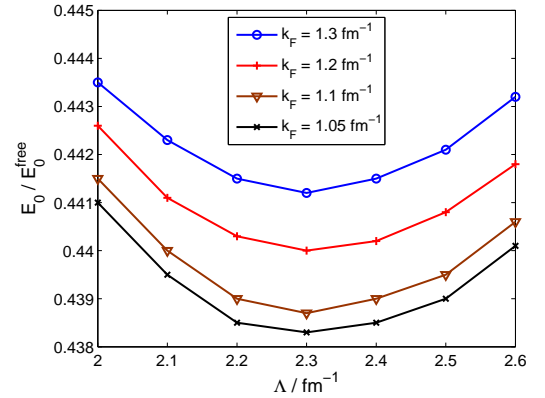


FIG. 6: Determination of the fixed point where $dE_0/d\Lambda = 0$ for CD-Bonn- ∞ .

Of great significance is the ratio of the ground state energy to that of the non-interacting case, namely E_0/E_0^{free} . At the unitary limit, it is expected to be an universal constant, named ξ . This constant is of great importance as it determines the equation of state of all low-density cold Fermi gas. At the unitary limit, our data on E_0/E_0^{free} all lie within a narrow window from 0.437 to 0.448. Such result confirms a universality over Fermion density in a wide range $(1.73 - 11.40) \times 10^{-2} fm^{-3}$. Most importantly, the numerical value of ξ is remarkably close

to that from Monte Carlo methods, which by far is believed to be the best estimate. Astra *et. al.* obtained 0.42(1) based on a square well potential and particle density $nR_0^3 = 10^{-6}$ (where R_0 is the potential range). Carlson *et. al.* obtained 0.44(1) based on a ‘cosh potential’, and particle density $n\mu^{-3} = 0.020$ (where $2/\mu$ is the effective range). In our case, $n\Lambda^{-3} = (1.4 - 9.4) \times 10^{-3}$ (where $\Lambda = 2.3\text{fm}^{-1}$ is the decimation scale in the renormalization). These works, including ours, employ very different interactions and various particle densities. Still, the value of ξ agrees incredibly well.

In Figure 4 we contrast the data from CD-Bonn- ∞ with that from the original CD-Bonn and other tuned potentials. Even though the 1S_0 scattering length in the original CD-Bonn is already fairly large ($a_s = -18.97\text{fm}$), still the equation of state, as predicted from the ratio E_0/E_0^{free} , has significant difference from the unitary limit. As seen in our data with CD-Bonn- ∞ potential, at the unitary limit the ratio $E_0/E_0^{free} = 0.44$ is practically independent of the underlying neutron density n .

C. Comparison with G-matrix results

As discussed in section II, our ring-diagram calculations are based on a model space framework. A model-space is defined by momentum $\{k \leq \Lambda\}$ where Λ is the decimation scale. The space with $k > \Lambda$ is integrated out, resulting in a model-space effective interaction V_{eff} . We have used so far the energy-independent V_{low-k} for V_{eff} . Alternatively, one can also use the energy-dependent G^M -matrix (of section II) as V_{eff} . These two approaches are formally equivalent. We have carried out calculations to check this equivalence.

We have repeated the ring diagram summation with the energy-independent V_{low-k} replaced by the energy-dependent model-space Brueckner G^M -matrix, and carry out a fully self-consistent computation in summing up the *pphh* ring diagrams. The exact procedures in Ref.[37] are followed (section II). Ring diagrams within a model space up to a cut-off momentum Λ is summed to all orders. We found that the ground state energy is rather insensitive to the choice of Λ . See Figure 7 for the data of CD-Bonn- ∞ and CD-Bonn(-18.97), done with $\Lambda = 2.3\text{fm}^{-1}$, 2.25fm^{-1} respectively. As illustrated, the two methods, namely, ring diagram summation with V_{low-k} and that with G^M -matrix, are fully consistent. This is a remarkable and reassuring result, as the calculational procedures of them are vastly different. For the G^M case, the s.p. spectrum, the RPA amplitudes Y and energies ω_m^- are all calculated self-consistently, while for the V_{low-k} case no such self-consistent procedures are needed. Clearly the V_{low-k} ring-diagram method is more desirable.

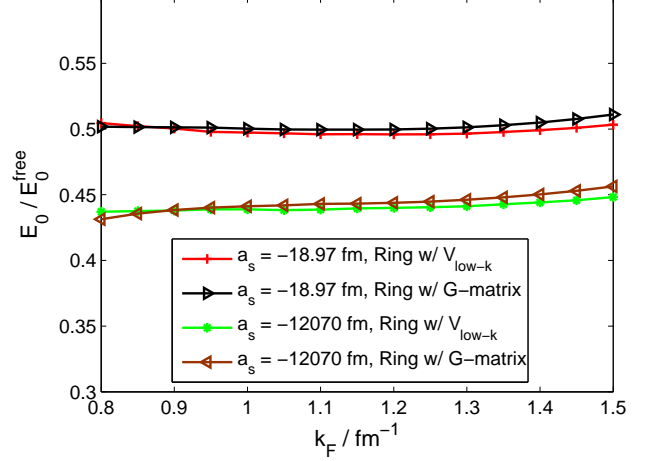


FIG. 7: The ratio E_0/E_0^{free} for the potentials CD-Bonn- ∞ and CD-Bonn(-19.87) computed with two methods. Ring w/ G -mat: *pphh* ring diagrams summation with Brueckner G^M -matrix. $\Lambda = 2.3\text{fm}^{-1}$ is used, computation is fully self-consistent. Ring w/ V_{low-k} : *pphh* ring diagrams summation with V_{low-k} , fixed point is at $\Lambda = 2.3$.

D. Schematic effective interaction at unitary limit

At the unitary limit, the simple equation of state $E_0 = \xi E_0^{free}$ in neutron matter suggests a very counter-intuitive nature in the underlying system: strongly interacting fermions essentially can be described by a non-interacting picture with an effective mass. This unexpected ‘simplicity’ can best be captured by a schematic interaction. To illustrate this, let us consider neutron matter confined in a closed Fermi sea $|\Phi_0(k_F)\rangle$. In other words, we consider neutron matter in a one-dimensional model space. We denote the effective interaction for this model space as V_{FS} . Then the potential energy per particle is

$$\begin{aligned} \frac{PE}{A} &= \langle \Phi_0(k_F) | V_{FS} | \Phi_0(k_F) \rangle / A \\ &= \frac{8}{\pi} \int_0^{k_F} \left(1 - \frac{3k}{2k_F} + \frac{k^3}{2k_F^3} \right) \langle k | V_{FS} | k \rangle k^2 dk \end{aligned} \quad (19)$$

where k is the relative momentum.

Suppose we take V_{FS} as a contact effective interaction

$$V_{FS} = \frac{1}{\frac{S}{a_s} - \frac{2}{\pi} k_F} \quad (20)$$

($\hbar = m = 1$) where S is a positive parameter with $S \ll |a_s|$. When $S=1$ and k_F replaced by Λ , V_{FS} is the same the effective interaction for the pion-less effective field theory [34, 35]. Substituting the above into Eq.(19) gives

$$\xi = 1 + \frac{5}{9} \frac{1}{\frac{\pi}{2} \frac{S}{a_s k_F} - 1}. \quad (21)$$

At the unitary limit (infinite a_s), the above gives $\xi=4/9$, independent of k_F , which is practically the same as the result for $\xi(-12070)$ of Fig. 4. The above also gives ξ for finite a_s . At the unitary limit, we expect V_{FS} to be unique. For finite a_s (away from the unitary limit), it is not expected to be unique and the parameter S is expected to depend on the underlying potential. As shown in Fig. 4, we have calculated ξ using the CD-Bonn potentials of finite scattering lengths. These results can also be qualitatively described by the above equation. For instance, for $S = 1.25$ and $k_F = 1.0$, the above equation gives $\xi = 0.54, 0.50$ and 0.39 respectively for $a_s = -9.87 fm, -18.97 fm$ and $+21.01 fm$. In short, certain main features of our results obtained from ring-diagram calculations with the CD-Bonn potentials can be qualitatively reproduced by the above simple contact effective interaction.

V. SUMMARY

In conclusion, we have carried out a detailed study on neutron matter at and close to the unitary limit with a low-momentum ring diagram approach. By slightly tuning the realistic CD-Bonn potential, we have obtained 1S_0 neutron potentials of specific scattering lengths, in particular the CD-Bonn- ∞ one with a_s of $-12070 fm$. By integrating out their momentum components beyond a decimation scale Λ , we obtain renormalized low-

momentum interactions V_{low-k} of the same specific scattering lengths. The ground state energy E_0 of neutron matter are then calculated by summing up the $pphh$ ring diagrams to all orders within the model space $\{k < \Lambda\}$. A fixed-point criterion is used to determine the decimation scale Λ . We have carried out ring-diagram calculations using two types of renormalized interactions, the energy-independent V_{low-k} and the energy-dependent G -matrix, with results given by them being nearly identical. The V_{low-k} ring-diagram method has a simpler formalism and is also more suitable for numerical calculation. For the CD-Bonn- ∞ potential, the ratio E_0/E_0^{free} is found to be very near a universal constant of 0.44 over the neutron density range $(1.73 - 11.40) \times 10^{-2} fm^{-3}$. Our result agrees well with the recent experimental measurement and Monte-Carlo computation on cold Fermi gas at the unitary limit.

Acknowledgement We thank G.E. Brown, E. Shuryak, T. Bergmann and A. Schwenk for many helpful discussions. This work is supported in part by U.S. Department of Energy under grant DF-FG02-88ER40388, and by the U.S. National Science Foundation under Grant PHY-0099444.

-
- [1] R. F. Bishop, Int. J. Mod. Phys. B **15**, iii (2001), Many-Body Challenge Problem by G. F. Bertsch.
 - [2] C. A. Regal and D. S. Jin, Phys. Rev. Lett. **90**, 230404 (2003); S. Jochim, M. Bartenstein, G. Hendl, J. Hecker Denschlag, R. Grimm, A. Mosk, M. Weidemüller, Phys. Rev. Lett. **89**, 273202 (2002); C. H. Schunck, M. W. Zwierlein, C. A. Stan, S. M. F. Raupach, W. Ketterle, A. Simoni, E. Tiesinga, C. J. Williams, and P. S. Julienne, Phys. Rev. A **71**, 045601 (2005).
 - [3] S. Stringari, Europhys. Lett. **65**, 749 (2004).
 - [4] A. Bulgac and G. F. Bertsch, Phys. Rev. Lett. **94**, 070401 (2005).
 - [5] H. Heiselberg, Phys. Rev. Lett. **93**, 040402 (2004).
 - [6] J. Kinast, S.L. Hemmer, M.E. Gehm, A. Turlapov, and J.E. Thomas, Phys. Rev. Lett. **92**, 150402 (2004).
 - [7] J. Kinast, A. Turlapov, and J. E. Thomas, Phys. Rev. A **70**, 051401(R) (2004).
 - [8] A. Altmeyer, S. Riedl, C. Kohstall, M. J. Wright, R. Geursen, M. Bartenstein, C. Chin, J. Hecker Denschlag, and R. Grimm, Phys. Rev. Lett. **98**, 040401 (2007).
 - [9] M.J. Wright, S. Riedl, A. Altmeyer, C. Kohstall, E.R. Sánchez Guajardo, J. Hecker Denschlag, and R. Grimm, Phys. Rev. Lett. **99**, 150403 (2007).
 - [10] A. Bulgac, Phys. Rev. Lett. **95**, 140403 (2005).
 - [11] A. Bulgac, Joaquín E. Drut, and Piotr Magierski, Phys. Rev. Lett. **96**, 090404 (2006).
 - [12] A. Bulgac, Joaquín E. Drut, and Piotr Magierski, Phys. Rev. Lett. **99**, 120401 (2007).
 - [13] J. E. Thomas, J. Kinast, and A. Turlapov, Phys. Rev. Lett. **95**, 120402 (2005).
 - [14] G. A. Baker, Jr., Phys. Rev. C **60**, 054311 (1999).
 - [15] H. Heiselberg, Phys. Rev. A **63**, 043606 (2001).
 - [16] G. M. Bruun, Phys. Rev. A **70**, 053602 (2004).
 - [17] A. Perali, P. Pieri, and G. C. Strinati, Phys. Rev. Lett. **93**, 100404 (2004).
 - [18] Y. Nishida, and D. T. Son, Phys. Rev. Lett. **97**, 050403 (2006).
 - [19] R. Haussmann, W. Rantner, S. Cerrito, and W. Zwerger, Phys. Rev. A **75**, 023610 (2007).
 - [20] J.-W. Chen, and E. Nakano, Phys. Rev. A **75**, 043620 (2007).
 - [21] J. Carlson, S.-Y. Chang, V. R. Pandharipande, and K. E. Schmidt, Phys. Rev. Lett. **91**, 050401 (2003).
 - [22] G. E. Astrakharchik, J. Boronat, J. Casulleras, and S. Giorgini, Phys. Rev. Lett. **93**, 200404 (2004).
 - [23] T. Bourdel, L. Khaykovich, J. Cubizolles, J. Zhang, F. Chevy, M. Teichmann, L. Tarruell, S. J. J. M. F. Kokkelmans, and C. Salomon, Phys. Rev. Lett. **93**, 050401 (2004).
 - [24] J. Kinast, A. Turlapov, J. E. Thomas, Q. Chen, J. Stajic, and K. Levin, Science **307**, 1296 (2005).
 - [25] G. B. Partridge, W. Li, R. I. Kamar, Y.-A. Liao, and R. G. Hulet, Science **311**, 503 (2006).
 - [26] J. T. Stewart, J. P. Gaebler, C. A. Regal, and D. S. Jin,

- Phys. Rev. Lett **97** 220406 (2006).
- [27] A. Schwenk and C. J. Pethick, Phys. Rev. Lett. **95**, 160401 (2005).
 - [28] D. Lee and T. Schäfer, Phys. Rev. C **73**, 015202 (2006).
 - [29] R. Machleidt, Phys. Rev. C **63**, 024001 (2001).
 - [30] S.K. Bogner, T.T.S. Kuo and L. Coraggio, Nucl. Phys. **A684**, 432 (2001).
 - [31] S.K. Bogner, T.T.S. Kuo, L. Coraggio, A. Covello and N. Itaco, Phys. Rev. C **65**, 051301R (2002).
 - [32] L. Coraggio, A. Covello, A. Gargano, N. Itako, T.T.S. Kuo, D.R. Entem and R. Machleidt, Phys. Rev. C **66**, 021303(R) (2002).
 - [33] A. Schwenk, G.E. Brown and B. Friman, Nucl. Phys. **A703**, 745 (2002).
 - [34] S.K. Bogner, T.T.S. Kuo and A. Schwenk, Phys. Rep. **386**, 1 (2003).
 - [35] T. Schäfer, C.-W. Kao, S.R. Cotanch, Nucl. Phys. **A762**, 82 (2005).
 - [36] J.D. Holt, T.T.S. Kuo and G.E. Brown, Phys. Rev. C **69**, 034329 (2004).
 - [37] H.Q. Song, S.D. Yang and T.T.S. Kuo, Nucl. Phys. **A462**, 491 (1987).
 - [38] H. A. Bethe, Annu. Rev. Nucl. Sci. **21**, 93 (1971).
 - [39] J.W. Holt and G.E. Brown, p.239 in Hans Bethe and His Physics (World Scientific, July 2006, edited by G.E. Brown and C.-H. Lee).
 - [40] R. B. Wiringa, V.G.J. Stoks and R. Schiavilla, Phys. Rev. C **51**, 38 (1995).
 - [41] V.G.J. Stoks, R.A.M. Klomp, C.P.F. Terheggen and J.J. de Swart, Phys. Rev. C **49**, 2950 (1994).
 - [42] D.R. Entem, R. Machleidt, Phys. Rev. C **68**, 041001 (2003).
 - [43] K. Suzuki and S. Y. Lee, Prog. Theor. Phys. **64**, 2091 (1980).
 - [44] F. Andreozzi, Phys. Rev. C **54**, 684 (1996).
 - [45] G.E. Brown, M. Rho, Phys. Rev. Lett. **66**, 2720 (1991).
 - [46] G.E. Brown, M. Rho, Phys. Rept. **396**, 1 (2004).
 - [47] R. Rapp, R. Machleidt, J.W. Durso and G.E. Brown, Phys. Rev. Lett. **82**, 1827 (1999).